KONA Powder and Particle Journal No. 34 (2017) 80–90/Doi:10.14356/kona.2017009 Original Research Paper

# Synthesis of Nanoparticles by Laser Ablation: A Review †

**Myungjoon Kim [1], Saho Osone [2], Taesung Kim [1,3], Hidenori Higashi [2] and Takafumi Seto [2]***

[1] *School of Mechanical Engineering, Sungkyunkwan University, Korea*
[2] *Faculty of Natural System, Kanazawa University, Japan*
[3] *SKKU Advanced Institute of Nano Technology (SAINT), Sungkyunkwan University, Korea*

**Abstract**

Laser ablation is a method for fabricating various kinds of nanoparticles including semiconductor quantum dots, carbon nanotubes, nanowires, and core shell nanoparticles. In this method, nanoparticles are generated by nucleation and growth of laser-vaporized species in a background gas. The extremely rapid quenching of vapor is advantageous in producing high purity nanoparticles in the quantum size range (< 10 nm). In this review, the formation mechanism of nanoparticles by laser ablation is summarized. Recent progress on the control of nanoparticle size and the challenges for functional nanoparticle synthesis by advanced laser ablation technology are then discussed.

**Keywords:** laser ablation, nanoparticle, quantum dot, nanocarbons

## 1. Introduction

Nanoparticles have a variety of unique properties that are not observable in bulk materials (Buzea et al., 2007). The most critical characteristic of nanoparticles is that the properties (electrical, optical, magnetic, and so on) depend strongly on the size and size distribution of the particles (Kim et al., 2014). For example, silicon nanoparticles are photoluminescent in the visible spectrum at room temperature (Kenemitsu, 1995; Yoshida et al., 1998); the wavelength of the emitted light can be controlled with the particle size (Orii et al., 2003a). Nano-sized titania particles have also gathered attention as building blocks for photovoltaic devices (O'regan and Gratzel, 1991) and for photocatalytic applications (Fujishima and Honda, 1972). The photochemical properties of titania nanoparticles also have a strong dependence on particle size as well as on crystal structure. Many kinds of nanoparticles exhibit special characteristics (ferromagnetism, paramagnetism, pinned emission, fluorescence, spin quantum effect, etc.) when the size of a particle is at the nanoscale level (Zheng et al., 2004; Kim et al., 2011; Kim et al., 2014). The special characteristics are significantly impacted by the size and size distribution of the particles.

Various nanoparticle fabrication methods have been developed with the bottom-up approach in the liquid phase (including sol-gel and chemical reduction) as well as vapor phase (such as physical/chemical vapor deposition and flame synthesis). Each fabrication method has advantages and disadvantages. Liquid phase methods are cost-effective and are used for synthesizing various kinds of nanoparticles with well-controlled structures at the laboratory scale. Vapor phase processes are superior at synthesizing high purity nanoparticles by means of the continuous flow reactor. In both of the liquid and gas bottom-up processes, solid nanoparticles are generated from the nucleation of supersaturated species that are prepared by precursor reactions and/or evaporation of solids. Laser ablation is a method that utilizes laser (which is an acronym for light amplification by stimulated emission of radiation) as an energy source for ablating solid target materials. In this process, extremely high energy is concentrated at a specific point on a solid surface to evaporate light-absorbing material. The term 'ablation' refers to the removal of surface atoms and involves not only a single photon process (breaking the chemical bonds) but also multiphoton excitation (thermal evaporation). High-purity nanoparticles can be generated by laser ablation because the purity of the particles is basically determined by the purity of the target and ambient media (gas or liquid) without contamination from the reactor. However, it is difficult to control size distribution, agglomeration, and

† Received 25 January 2016; Accepted 22 March 2016
J-STAGE Advance Publication online 30 April 2016
[1,3] 300 Cheoncheon-dong, Jangan-gu, Suwon, Gyeonggi, 440-746, Korea
[2] Kakuma-machi, Kanazawa, Ishikawa 920-1192, Japan
* Corresponding author: Takafumi Seto;
E-mail: t.seto@staff.kanazawa-u.ac.jp
TEL: +81-76-234-4815 FAX: +81-76-264-6239

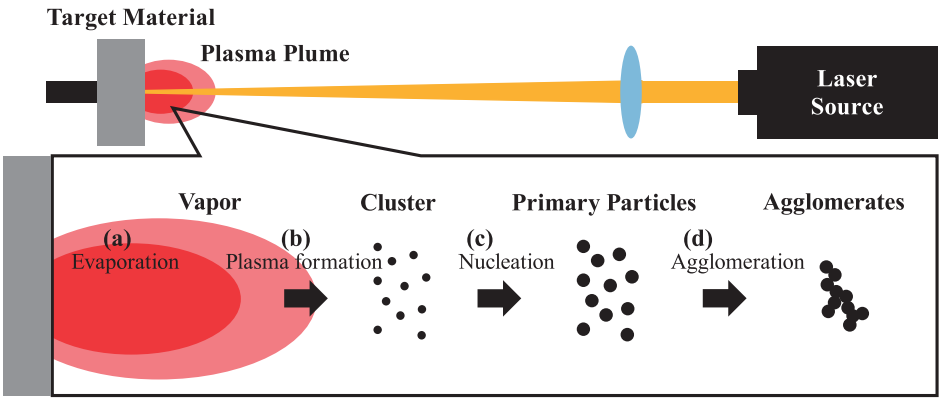


**Fig. 1** Schematic of particle generation procedure in the laser ablation process.

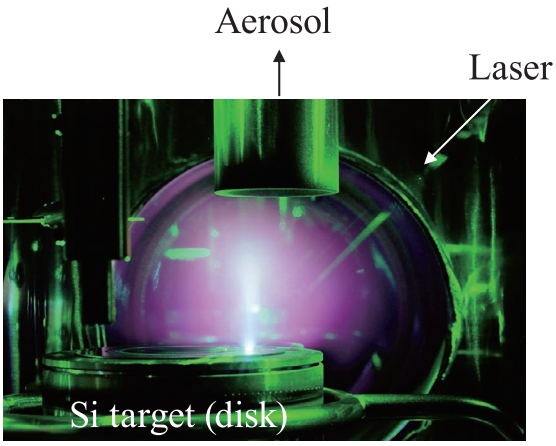


**Fig. 2** Laser-induced plume of silicon in low pressure.

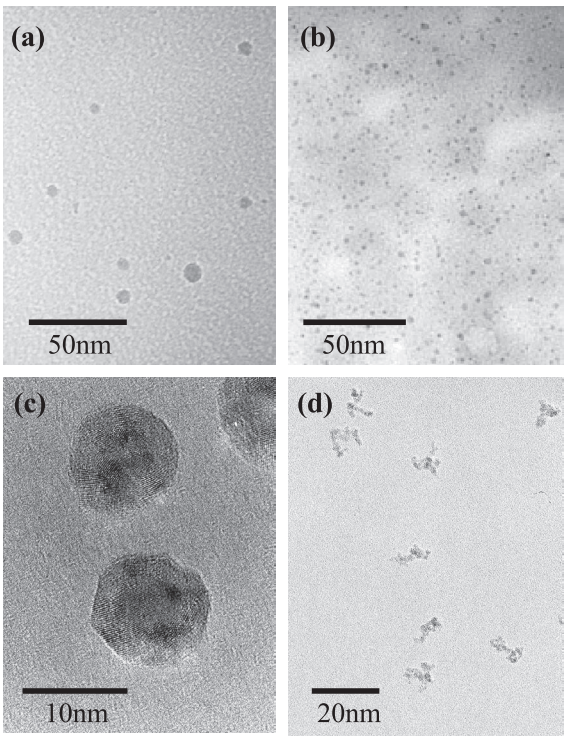


**Fig. 3** Typical transmission electron micrographs of laser ablation-generated **(a)** silicon, **(b)** carbon and **(c)** surface-oxidized nickel nanoparticles. **(d)** Aggregates of nickel nanoparticles as a result of coagulation and necking.

crystal structure in the conventional laser ablation process since nanoparticles are built by random (Brownian) motion of molecules. Therefore, several advanced laser ablation techniques have been developed for fabricating morphology-controlled nanoparticles. In this review, laser ablation-based nanoparticle formation processes and their mechanisms are briefly discussed, followed by a review of recent studies of laser ablation techniques for synthesizing various kinds of nanoparticles. Finally, advanced laser ablation processes for synthesizing functional nanomaterials with highly controlled nanostructures are introduced.

## 2. Nanoparticle formation by laser ablation

### 2.1 Basic concept of laser ablation

**Fig. 1** is a schematic of the nanoparticle formation process by laser ablation. When the laser beam is focused on the surface of a solid target material in the ambient media (gas or liquid), the temperature of the irradiated spot rapidly increases, vaporizing the target material. The collisions between the evaporated species (atom and clusters) and the surrounding molecules result in excitation of the electron state coupled with light emission and generation of electrons and ions, forming a laser-induced plasma plume (**Fig. 2**). The plasma structures (size of the plume and its emission spectrum) depend on the target material, ambient media (liquid or gas), ambient pressure, and laser conditions. **Fig. 3** shows typical transmission electron micrographs of nanoparticles generated by laser ablation of various materials. In general, laser ablation in low-pressure background gas is preferable for creating a large plume and works well in generating small particles (**Fig. 3(a)**).

Laser ablation in liquid is employed to confine the plasma plume in a small region to directly disperse nanoparticles in the liquid phase (**Fig. 3(b)**). In any case, the ambient media must be carefully selected because the laser-generated particles easily react with surrounding molecules to create complexes such as oxides and other undesirable species (**Figs. 3(b)** and **(c)**). Coagulation is another critical phenomena that must be finely controlled in the later stages of nanoparticle formation. Since laser-generated particles have a very clean surface, agglomerated particles create chemical bonds at the contact point (neck), which significantly compromise the properties of primary particles (**Fig. 3(d)**, Sakiyama et al., 2004). The low-pressure gas process is advantageous not only for reducing the size of the primary particles but also for preventing coagulation.

## 2.2 Laser

For the fabrication of nanoparticles of the desired size and structure, the selection of a suitable laser system is one of the most critical decisions. The evaporation rate of the target material is generally determined by the laser parameters (laser source, wavelength, fluence, pulse width and frequency), the light absorption efficiency of the target material, and the condition of the ambient media. Laser energy per unit area on the target material is defined as fluence of the laser $F$, which is given as,

$$F = \frac{I}{A} \tag{1}$$

where $I$ [J/pulse] is the laser power and $A$ [m$^2$] is the area of the laser spot. In the case of silicon nanoparticle formation using the double harmonic wave of the Nd:YAG laser (wavelength of 532 nm), a laser with a fluence ($F$) of more than several J/cm$^2$ is frequently used. The wavelength of the laser is another important parameter that determines the absorption efficiency of the target. The absorption depth and spot (focusing) area are also influenced by laser wavelength (Friedrich et al., 1998). In early studies of nanoparticle synthesis by laser ablation, excimer lasers in the ultraviolet spectrum (193 nm for ArF, 248 nm for KrF) are often used as a light source (Yoshida et al., 1996; Shinde et al., 2000). Recently, Q-switch pumped pulsed YAG (Yttrium Aluminum Garnet) lasers are more commonly used for laser ablation because they do not require hazardous gases. The wavelength of Nd:YAG laser (1,064 nm for fundamental wave) can be changed by employing nonlinear optical crystals. For example, 532 nm for second harmonic generation and 355 nm for third harmonic and other frequency mixing are possible. Overall, it is difficult to attain stable ablation using the fundamental wave because of the weaker light absorption in the infrared region (Lu et al., 2008). Torrisi et al. (2003) investigated the effect of wavelength on laser ablation of solid Cu using a 1064 nm Nd:YAG laser and a 308 nm XeCl excimer laser. They showed that UV laser is more efficient at evaporating the copper atoms, even though infrared radiation has higher ionic kinetic energy and higher plasma temperature. Lu et al. (2008) calculated the evaporation thresholds of Si and estimated them to be $2 \times 10^{10}$ W/cm$^2$ for a 266 nm wavelength laser and $4 \times 10^{11}$ W/cm$^2$ for a 532 nm wavelength laser. Short pulse lasers (nanoseconds) with less energy density have also been used to generate Si nanoparticles. As an example, Seto et al. (2001b) generated Si nanoparticles with a 5 ns pulsed Nd:YAG laser (532 nm) with an average fluence of 16 J/cm$^2$ (about $3 \times 10^9$ W/cm$^2$). The pulse width of the laser is also another important parameter that determines peak energy. Recently picosecond (Lau et al., 2014) and femtosecond lasers (Fischer et al., 2015) have been applied to enhance the photon absorption efficiency of the target surface to break chemical bonding.

## 2.3 Change in the temperature by laser irradiation

When the target surface is irradiated with short laser pulses, the absorbed photon energy is transferred to the solid lattice as a form of thermal (internal) energy. Heat transfer in the electron and lattices subsystems can be characterized by the following one-dimensional, two-temperature diffusion equations with temperatures of electron $T_e$ and lattices $T_i$ (Chichkov et al., 1996).

$$C_e \frac{\partial T_e}{\partial t} = -\frac{\partial Q(z)}{\partial z} - \gamma(T_e - T_i) + S \tag{2}$$

$$C_i \frac{\partial T_i}{\partial t} = \gamma(T_e - T_i) \tag{3}$$

$$Q(z) = -k_e \frac{\partial T_e}{\partial z}, \qquad S = I(t) A \alpha \exp(-\alpha z) \tag{4}$$

where $C_e$ and $C_i$ are the heat capacities of the electron and lattices subsystems, $z$ is perpendicular direction to the heat surface, $Q(z)$ is the heat flux, $\gamma$ is the electron-phonon coupling strength, $S$ is the laser source term, $k_e$ is the heat conductivities of the electron, $I(t)$ is the laser intensity, $A$ is the absorbance of the sample, and $1/\alpha$ can be defined as the optical penetration depth.

Equations (2–4) can be modified for the laser pulse width. In the case of nanosecond laser pulses, $T_e$ is assumed to be equal to $T_i$ (Chichkov et al., 1996) due to the duration of the laser pulse being much larger than the lattice heating time. Then equations (2–4) can be reduced to

$$C_i \frac{\partial T_i}{\partial t} = \frac{\partial}{\partial z}\left(k_o \frac{\partial T}{\partial z}\right) + I(t) A \alpha \exp(-\alpha z) \tag{5}$$

where, $k_o$ is the conventional equilibrium thermal conduc-

tivity of a substance.

### 2.4 Nucleation and particle growth

Since the laser-vaporized materials are very rapidly quenched from extremely high temperatures (> 5000 K) to room temperature (usually shorter than 50 μs after the laser pulse; Wen at al., 2006), nanometer-sized particles form by supersaturated vapor nucleation at the edge of the laser plume (**Fig. 1(c)**). The change in the number concentration of vaporized material (monomer), clusters, and particles can be given by the general dynamic equation (Pratsinis and Kim, 1989) by considering nucleation, condensation, and coagulation. Numerical simulations of the solutions to the general dynamic equation have been conducted for predicting the size distribution of nanoparticles generated by the ablation process (Wen et al., 2007; Kuroda et al., 2012). It should be noted that there are significant contributions of electron and ion species on the nucleation process, *i.e.* ion-induced nucleation in the laser ablation process. As a result, the particles generated by the laser ablation were electrically charged (Seto et al., 2003). However, it is still difficult to reproduce the rapid change in the size distribution due to nucleation and growth of the laser-vaporized materials. To experimentally analyze the particle formation process, advanced in-situ observation techniques are necessary. Emission spectroscopy of plumes (Geohegan et al., 1998) is one in-situ measurement technique for investigating the dynamics of particle formation. The mobility analyzing technique may also be applied to investigate the effect of particle generation conditions on the size distribution as discussed later in this review.

## 3. Synthesis of various kinds of nanoparticles by laser ablation

### 3.1 Semiconductor quantum dot

A semiconductor quantum dot is a nanocrystal that exhibits quantum properties such as tunable light emission driven by the quantum confinement effect (Canham, 2000) and single electron transport phenomena (Tilke et al., 2001). There are some reports on the synthesis of II–VI and III–V semiconductor quantum dots by laser ablation such as formation of GaAs nanocrystals (Perriere et al., 2001), ZnSe and CdS quantum dots (Anikin et al., 2002), CdSe and CdTe nanoparticles (Ruth and Young, 2006) that can be applied to the study of optical imaging therapy (Wolfbeisref, 2015). However, the laser ablation process for composite materials is challenged in controlling the stoichiometry and crystallinity in the process for rebuilding laser-vaporized elements. Group-IV elements such as silicon and germanium and carbon nanoparticles are single element semiconductors. Silicon and carbon are abundant (non-rare metal) elements that exhibit a variety of unique properties when the particle sizes are in the nanometer range. Therefore, we will focus on the synthesis of silicon and carbon nanoparticles in this review.

**Table 1** lists laser ablation studies on silicon nanoparticle synthesis. Okada and Iijima (1991) measured the oxidation rate of silicon nanoparticles generated by laser ablation and found that the oxidation rate drops with decreasing particle size. They used a YAG laser of 12 millisecond pulse width and produced 20–500 nm particles under pressures of 0.75 to 3 Pa. Yoshida et al. (1996) synthesized silicon crystallites in gas between pressures of 333 to 1330 Pa using an argon-fluoride (ArF) excimer laser (193 nm wavelength, 12 ns pulse width, fluence 1 J/cm$^2$). They showed mean diameter of particle can be varied as a function of the He background gas pressure. The mean diameter calculated from the SEM images were about 23 nm at 333 Pa, 36 nm at 432 Pa, and 52 nm at 665 Pa. Pressure effects on particle size in laser ablation generation was studied in more detail by Seto et al. (2003) through particle classification with a low pressure differential mobility analyzer (low pressure DMA, LPDMA, see later section). Suzuki et al. (2001) investigated the suitability of LPDMA as a size classification tool for the silicon nanoparticles generated by laser ablation under low-pressure conditions. They compared the mode size and the geometrical standard deviation (GSD) of silicon nanoparticles with and without LPDMA size classification. The GSD was significantly reduced from 1.6 (as-prepared) to 1.2 for particles as small as 4 nm after classification by LPDMA. The results indicate that size classification is effective for generating the monodispersed nanoparticles that can be used to clarify the relationship between quantum properties and size.

Another important factor affecting the quantum properties of Si nanoparticles is their crystallinity. Unfortunately, laser ablation tends to generate amorphous agglomerates which have poor (broad) optical properties (Hirasawa et al., 2004). Gas phase annealing is an effective method to improve crystallinity and the shape of the Si nanoparticles. **Fig. 4** shows laser ablation process coupled with gas phase annealing, particle classifying, and particle measurement systems. Since laser ablation systems have good compatibility with gas flow reactors and other instruments as shown in **Fig. 4**., particle morphologies (size, shape and crystallinity etc.) can be controlled in the aerosol phase. Hirasawa et al. (2004) investigated the change in the crystallinity of Si nanoparticles by Raman spectroscopy and TEM as a function of the gas-phase annealing temperature. They also employed LPDMA for size selection and studied the size-dependent crystalli-

**Table 1** Silicon nanoparticle synthesis studies using pulsed laser ablation method (A: annealing, m: mean, M: mode)

| Author | Laser Source | Pressure | Additional Process | Particle | Particle size |
|---|---|---|---|---|---|
| Okada and Iijima 1991 | YAG | 0.75~3.0 Pa | | | 20~500 nm |
| Yoshida et al. 1996 | ArF excimer | 333~1330 Pa | | | 3~100 nm |
| | | 333 Pa | | Aggregates | (m) 23 nm |
| | | 434 Pa | | Aggregates | (m) 36 nm |
| | | 666 Pa | | Aggregates | (m) 52 nm |
| Seto et al. 2001a | Nd:YAG | 666 Pa | DMA | Primary | 2~7 nm |
| Seto et al. 2001b | Nd:YAG | 666 Pa | DMA | Primary | (M) 7, 10 nm |
| Suzuki et al. 2001 | Nd:YAG | 666 Pa | | Primary | (M) 6 nm |
| | | 666 Pa | DMA | Primary | (M) 3.8 nm |
| Seto et al. 2003 | Nd:YAG | 333 Pa | | Aggregates | ~70 nm |
| | | 666 Pa | | Aggregates | ~ 120 nm |
| | | 280 Pa | DMA | Primary | (M) 5 nm |
| | | 334 Pa | DMA | Primary | (M) 4 nm |
| | | 380 Pa | DMA | Primary | (M) 4 nm |
| | | 380 Pa | DMA | Aggregates | (M) > 6 nm |
| | | 434 Pa | DMA | Primary | (M) 4 nm |
| | | 434 Pa | DMA | Aggregates | (M) > 6 nm |
| Orii et al. 2003a | Nd:YAG | 931 Pa | (A) 900 °C, DMA | Primary | (M) 3~6 nm |
| Orii et al. 2003b | Nd:YAG | 931 Pa | (A) 900 °C, DMA | Primary | (M) 6.9 nm |
| Hirasawa et al. 2004 | Nd:YAG | 1000 Pa | (A) 300 °C, DMA | Primary | (M) > 14 nm |
| | | 1000 Pa | (A) 500 °C, DMA | Primary | (M) 11.2 nm |
| | | 1000 Pa | (A) 700 °C, DMA | Primary | (M) 10.3 nm |
| | | 1000 Pa | (A) 900 °C, DMA | Primary | (M) 10 nm |
| Hirasawa et al. 2006 | Nd:YAG | 1000 Pa | DMA | Primary | 7~14 nm |

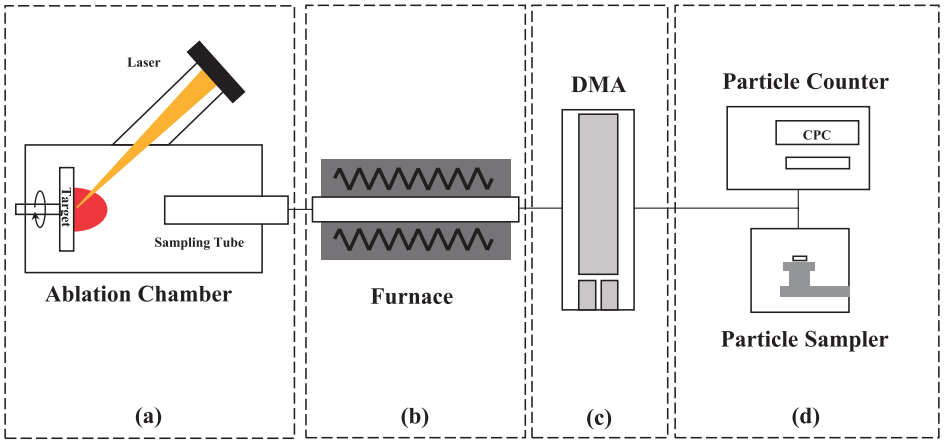


**Fig. 4** Schematic of nanoparticle synthesis process using laser ablation, which is composed of **(a)** particle generation, **(b)** gas phase annealing, **(c)** particle classifying, and **(d)** particle measurement.

zation process of Si nanoparticles in the gas phase. Based on their analysis, for Si nanoparticles (< 10 nm), gas phase annealing over 900 °C is effective in improving both crystallinity and shape as a result of sintering. The size-classified, spherical, and single crystal Si nanoparticles generated by the method exhibited sharp photoluminescence (PL) that was tunable with the size of Si nanoparticles (Orii et al., 2003a, b). The PL spectra of Si nanoparticles showed that peak energy increased from 1.34 to 1.79 eV with a drop in particle size from 7 to 3 nm, and full width at half maxi-

mum (FWHM) of the PL drops to approximately 0.22 eV as a result of size classification by the LPDMA.

### 3.2 Metal and oxide nanoparticles

Metal and metal oxide nanoparticles also display various unique features that have potential for electrical, magnetic, catalytic, and optical applications. Some studies on the synthesis of metal and metal oxide nanoparticles by laser ablation are listed in **Table 2**. Kawakami et al. (2002) produced gold nanoparticles by laser ablation under helium gas under pressures of 3 to 90 kPa. They generated a film by directly depositing the gold nanoparticles on the substrate by generating an aerosol-jet. The microstructure of the gold film changed from porous to high density with increasing pressure. As a result, the electrical resistivity of the film changed from $10^{-1}$ Ωcm (3 kPa) to $10^{-5}$ Ωcm (50 kPa). Dikovska et al. (2013) also synthesized silver nanoparticles by laser ablation under high vacuum conditions (~$10^{-5}$ torr). They investigated the influence of Nd:YAG laser wavelength on the size of generated particles. They reported that a shorter wavelength (266 nm) was better at generating smaller particles (4 nm in diameter) and that it exhibited surface plasmon resonance.

Magnetic nanoparticles from transition metals and metal alloys have also been synthesized by laser ablation. Since magnetic properties are strongly influenced by purity, crystallinity, and particle size of the nanoparticles, advanced laser ablation (**Fig. 4**) is significantly more capable of controlling nanoparticle morphologies. Sakiyama et al. (2004) fabricated Ni particles of a select size coated with a NiO shell with the laser ablation method. They also applied the aerosol process, i.e., LPDMA size classification, and gas phase annealing to improve Ni nanoparticle morphology. A Ni/NiO core shell structure was successfully generated by the oxidation of Ni nanoparticles. Seto et al. (2004, 2005) investigated the magnetic properties of Ni/NiO nanoparticles generated by this method using a superconducting quantum interference device (SQUID) magnetometer at room temperature. Ferromagnetism was observed with a film comprising nickel particles larger

**Table 2** Metallic nanoparticle synthesis studies using pulsed laser ablation method (A: annealing, m: mean, M: mode, S: shell thickness)

| Author | Laser Source | Material | Pressure | Additional Process | Particle | Particle size |
|---|---|---|---|---|---|---|
| Shinde et al. 2000 | Excimer | $Fe_xO_y$ | 266 Pa | Cold Finger | | 30~60 nm |
| | | SrM | 266 Pa | Cold Finger | | 15~100 nm |
| Seto et al. 2001a | Nd:YAG | $TiO_x$ | 2.6~13.3 kPa | DMA | Primary | 10~50 nm |
| Hirasawa et al. 2002 | Nd:YAG | $TiO_x$ | 1.73 kPa | DMA | Primary | (M) 5.9 nm |
| | | | 1.73 kPa | (A) 500 °C, DMA | Primary | (M) 4.9 nm |
| | | | 1.73 kPa | (A) 650 °C, DMA | Primary | (M) 4.4 nm |
| | | | 1.73 kPa | (A) 800 °C, DMA | Primary | (M) 6.9 nm |
| | | | 1.73 kPa | (A) 900 °C, DMA | Primary | (M) 14.3 nm |
| Harano et al. 2002 | Nd:YAG | $TiO_x$ | 101.3 kPa | | Aggregates | 10~50 nm, 100~1000 nm |
| Kawakami et al. 2002 | Nd:YAG | Au | 3 kPa | DMA | Primary | (M) 8 nm |
| | | | 7 kPa | DMA | Primary | (M) 13 nm |
| | | | 20 kPa | DMA | Primary | (M) 20 nm |
| | | | 30 kPa | DMA | Primary | (M) 30 nm |
| | | | 50 kPa | DMA | Primary | (M) 75 nm |
| | | | 90 kPa | DMA | Primary | (M) 80 nm |
| Sakiyama et al. 2004 | Nd:YAG | Ni/NiO | 1 kPa | DMA | Aggregates | |
| | | | 1 kPa | (A) 400~800 °C, DMA | Primary | 5~20 nm (S) 2 nm |
| Seto et al. 2006 | Nd:YAG | CoPt | 1 kPa | (A) 1000 °C, DMA | Primary | (M) 14 nm |
| Seto et al. 2007 | Nd:YAG | $CoPt/SiO_2$ | 1 kPa | (A) 1000 °C, DMA | Primary | (M) 7 nm, (S) 2 nm |
| Niu et al. 2012 | KrF excimer | FeNi | High vacuum | | Primary | (M) 4 nm |
| | | | 266 Pa | | Aggregates | (M) 6 nm |
| Dikovska et al. 2013 | Nd:YAG | Ag | ~$10^{-3}$ Pa | | Primary | (M) 4~11 nm |

than 6.2 nm in core diameter. In contrast, smaller Ni nanoparticles with core diameters of 3 nm exhibited superparamagnetism. They reported that the formation of an antiferromagnetic NiO shell is effective for controlling the manifestation of superparamagnetism in the nanometer-sized ferromagnetic Ni core.

Another approach for overcoming the superparamagnetic limit is to synthesize highly anisotropic magnetic alloy nanoparticles such as fct FePt and CoPt. Alloy nanoparticles of Co and Pt were synthesized by laser ablation by varying the Co:Pt ratio of the target (Seto et al., 2006). Their EDX results showed that the composition of the generated particles could be controlled by the target composition. The magnetization of the laser-synthesized CoPt particles (83.7 emu/g) was almost double that of bulk CoPt (44 emu/g). They also observed a weak exchange coupling at the interface between the ferromagnetic core (CoPt) and antiferromagnetic shell (CoO). Seto et al. (2007) also investigated the influence of shell material by synthesizing a non-magnetic $SiO_2$ shell by laser ablation of a multi-component target comprising Co, Pt and $SiO_2$. Metal oxide and metal composite nanoparticles have also been generated by laser ablation. Shinde et al. (2000) also synthesized iron oxides and strontium ferrite (SrM) with the laser ablation method and evaluated the magnetic characteristics.

Vapor phase synthesis of titania ($TiO_2$) nanoparticles has been extensively investigated since they have photovoltaic and photocatalytic applications (Harano et al., 2002; Pallotti et al., 2015). Seto et al. (2001a) synthesized $TiO_x$ particles by Nd:YAG laser ablation of a $TiO_2$ target in a background gas (He) with pressure ranging from 2.6 to 13.3 kPa. They observed increases in the mobility diameter due to agglomeration as the pressure increased. High-resolution TEM analysis of the nanostructures of the generated revealed that the metallic (Ti) core was covered with a sub-stoichiometric shell structure with a thickness of several nanometers. Hirasawa et al. (2002) also synthesized $TiO_x$ nanoparticles by laser ablation and investigated the effect of aerosol post-annealing temperatures of up to 900 °C. They reported an increase in the primary particle diameter due to sintering and change in crystallinity from amorphous form to anatase and rutile, which was confirmed by Raman scattering. They also discussed the non-stoichiometric phase of $TiO_x$ particles such as $Ti_2O_3$. More recently, Tsuji et al. (2012) investigated the effect of nucleation (particle formation) temperature on the morphology of $TiO_2$ nanoparticles generated by the laser oven process (laser ablation in a tubular furnace).

### 3.3 Nanocarbons and nanowires

The benefit of non-equilibrium laser ablation nucleation processes is that it can generate various kinds of crystal phases and allotropes that are not seen in the normal (equilibrium) synthesis processes. **Fig. 5** shows transmission electron micrographs of nanometer scale carbon allotropes (nanocarbons) such as carbon nanotubes (CNTs, **Fig. 5(a)**), onion-like carbon (**Fig. 5(b)**), and nanodiamonds (**Fig. 5(c)**) synthesized by laser ablation. Since laser ablation is superior at generating high-purity and nanometer-sized metal particles, it is also suitable as a catalyst for the growth of single walled carbon nanotubes (SWCNTs) on the substrate. For example, Kohno et al. (2004) generated Co/Mo and Co/Pt alloy nanoparticles by laser ablation and investigated the ethanol-CVD growth of the CNT on the substrate. In another development, laser ablation in a high temperature flow reactor (laser oven method) has been widely used to generate high-purity SWCNTs (Puretzky et al., 2000). References on carbon-related nanomaterial synthesis using gas-phase laser ablation are arranged in **Table 3**. Compared to conventional CVD formation on substrates, the laser oven method has an affinity for generating SWCNTs with low level of defects in a continuous flow-type generator.

As an example of nanocarbon generation in a flow-type generator, a simple and continuous one-step system using the laser oven method generated a SWCNT aerosol (Klanwan et al., 2010). A graphite target containing Ni and Co was ablated by pulsed laser in the tubular furnace

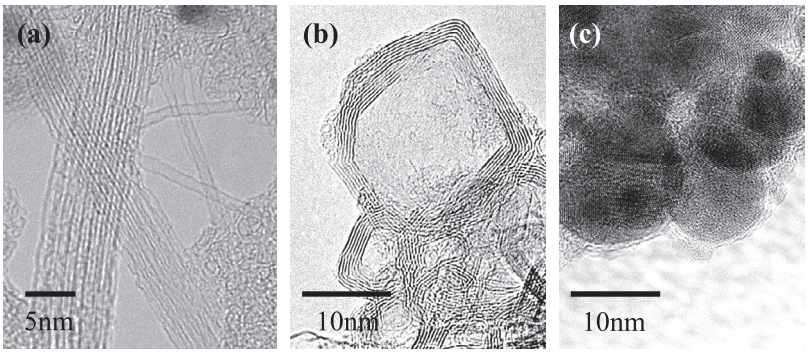


**Fig. 5** Transmission electron micrographs of nanocarbons generated by laser ablation. **(a)** Onion-like carbon, **(b)** carbon nanotubes, and **(c)** diamond-like nanoparticles.

at temperatures of 25 to 1080 °C. The generated SWCNTs (< 2 nm in diameter, **Fig. 5(a)**) were carried by atmospheric pressure nitrogen gas for on-line analysis of their size distribution using the scanning mobility particle sizer (SMPS). Other types of carbon allotropes have been synthesized by advanced laser ablation methods. Inoue et al. (2012) synthesized onion-like carbon nanoparticles (**Fig. 5(b)**) using a graphite target with a cavity that confined the generated particles so they can be irradiated by multiple laser beams. As a result of periodic laser beam irradiation of the gas-suspended carbon particles in the cavity, the phase transition from amorphous carbon nanoparticles to the orderly concentric graphitic shell structure was identified. Seto et al. (2014) also showed that the present method is capable of synthesizing a variety of unique nanostructured carbons including diamond-like carbon (**Fig. 5c**). They evaluated the change in the density of the carbon nanoparticles during the laser-induced phase transition.

## 4. Summary—Achieving large-scale production of nanoparticles by laser ablation

In this review, the formation mechanism and examples of nanoparticle synthesis by laser ablation were discussed. As mentioned previously, the properties of the nanoparticles depend strongly on size and size uniformity. Advanced laser ablation methods can generate size- and shape-controlled nanoparticles by post processing (**Fig. 4**), but that, at the same time, significantly reduces the production yield. In addition, laser ablation is disadvantaged by high input energy (Kushnir et al., 2008) and the small laser-irradiating area for evaporating the target materials. Therefore, laser ablation applications have been limited to exploring unique properties of new types of nanoparticles. To achieve large-scale production of nanoparticles by laser ablation, it is necessary to generate morphology-controlled nanoparticles without subsequent post-processing.

Laser ablation has an affinity for synthesizing anisotropic nanomaterials such as carbon nanotubes (Karthikeyan et al., 2009), nanorods (Tian et al., 2013) and nanowires (Rao et al., 2003) in the large-scale. In these processes, high-purity catalysts that are small in size and have good crystallinity play an important role in the anisotropic growth of such one-dimensional nanomaterials. In addition, laser ablation has good compatibility with aerosol flow systems and with the benefit of being capable of continuously producing large quantities of nanoparticles as well as nanoparticle-based nanomaterials. There are also several reports on the production of colloidal metal nanoparticles in a liquid flow system (Muttaqin et al., 2015). Such metal nanoparticles have applications as bio-markers.

Size classification by LPDMA is advantageous, not only for obtaining size-classified particles, but also for measuring the size distribution of nanoparticles in the gas phase process. Therefore, it can be implemented as a process monitor for optimizing process parameters (pressure, flow rate, temperature etc.). The size distribution of nanoparticles generated by laser ablation can be measured when an LPDMA is coupled with a particle detector such as an aerosol electrometer (Seto et al., 2001b). Quantum-sized particles (< 10 nm) with a relatively narrow size distribution can be generated by laser ablation under low pressure conditions without post-processing. For this purpose, an LPDMA/electrometer system can be used for exploring the optimum conditions to obtain nanoparticles with the desirable size distribution.

## Acknowledgements

The authors are grateful for support by JSPS KAKENHI Grant Number 15K14200.

**Table 3** Carbon nanoparticle synthesis studies using pulsed laser ablation method in a flow reactor (H: heating, D: diameter, L: length, M: mode)

| Author | Laser Source | Structure | Pressure | Additional Process | Size |
|---|---|---|---|---|---|
| Puretzky et al. 2000 | Nd:YAG<br>XeCl | SWNTs<br>SWNTs | 66.5 kPa<br>66.5 kPa | (H) 1000 °C<br>(H) 1000 °C | 200 nm/s growth rate |
| Klanwan et al. 2010 | Nd:YAG | SWNTs | 101.3 kPa | (H) 25~1080 °C | (D) < 2 nm, (L) > 500 nm |
| Inoue et al. 2012 | Nd:YAG | Amorphous<br>Onion-like | 101.3 kPa<br>101.3 kPa | Flat target<br>Cavity target | (M) 83 nm<br>(M) 18 nm |
| Seto et al. 2014 | Nd:YAG | Onion-like<br>Diamond-like | 101.3 kPa | Flat target<br>Cavity target | |

## References


Anikin K.V., Melnik N.N., Simakin A.V., Shafeev G.A., Voronov V.V., Vitukhnovsky A.G., Formation of ZnSe and CdS quantum dots via laser ablation in liquids, Chemical Physics Letters, 366 (2002) 357–360.

Buzea C., Pacheco I.I., Robbie K., Nanomaterials and nanoparticles: Sources and toxicity, Biointerphases, 2 (2007) MR17–MR71.

Chichkov B.N., Momma C., Nolte S., Von Alvensleben F., Tünnermann A., Femtosecond, picosecond and nanosecond laser ablation of solids, Applied Physics A, 63 (1996) 109–115.

Dikovska A.O., Alexandrov M.T., Atanasova G.B., Tsankov N.T., Stefanov P.K., Silver nanoparticles produced by PLD in vacuum: Role of the laser wavelength used, Applied Physics A, 113 (2013) 83–88.

Fischer D., Schwinghammer K., Sondermann C., Lau V.W., Mannhart J., Lotsch B.V., Laser ablation of molecular carbon nitride compounds, Applied Surface Science, 349 (2015) 353–360.

Friedrich C., Keynton R., Vasile M., Warrington R., Development of a core curriculum in miniaturization technologies, Journal of Engineering Education, 87 (1998) 567–574.

Fujishima A., Honda K., Electrochemical photolysis of water at a semiconductor electrode, Nature, 238 (1972) 37–38.

Geohegan D.B., Puretzky A.A., Duscher G., Pennycook S.J., Photoluminescence from gas-suspended SiOx nanoparticles synthesized by laser ablation, Applied Physics Letters, 73 (1998) 438–440.

Harano A., Shimada K., Okubo T., Sadakata M., Crystal phases of $TiO_2$ ultrafine particles prepared by laser ablation of solid rods, Journal of Nanoparticle Research, 4 (2002) 215–219.

Hirasawa M., Seto T., Orii T., Aya N., Shimura H., Synthesis of size-selected $TiO_x$ nanoparticles, Applied Surface Science, 197–198 (2002) 661–665.

Hirasawa M., Orii T., Seto T., Effect of insitu annealing on physical properties of Si nanoparticles synthesized by pulsed laser ablation, Applied Physics A, 79 (2004) 1421–1424.

Inoue A., Seto T., Otani Y., Onion-like carbon nanoparticles generated by multiple laser irradiations on laser-ablated particles, Carbon, 50 (2012) 1116–1122.

Kawakami Y., Seto T., Yoshida T., Ozawa E., Gold nanoparticles and films produced by a laser ablation/gas deposition (LAGD) method, Applied Surface Science, 197–198 (2002) 587–593.

Kim B.H., Lee N., Kim H., An K., Park Y.I., Choi Y., Shin K., Lee Y., Kwon S.G., Na H.B., Park J.-G., Ahn T.-Y., Kim Y.-W., Moon W.K., Choi S.H., Hyeon T., Large-scale synthesis of uniform and extremely small-sized iron oxide nanoparticles for high-resolution t1 magnetic resonance imaging contrast agents, Journal of the American Chemical Society, 133 (2011) 12624–12631.

Kim B.H., Hackett M.J., Park J., Hyeon T., Synthesis, characterization, and application of ultrasmall nanoparticles, Chemistry of Materials, 26 (2014) 59–71.

Klanwan J., Seto T., Furukawa T., Otani Y., Charinpanitkul T., Kohno M., Hirasawa M., Generation and size classification of single-walled carbon nanotube aerosol using atmospheric pressure pulsed laser ablation (AP-PLA), Journal of Nanoparticle Research, 12 (2010) 2747–2755.

Kohno M., Orii T., Hirasawa M., Seto T., Murakami Y., Chiashi S., Miyauchi Y., Maruyama S., Growth of single-walled carbon nanotubes from size-selected catalytic metal particles, Applied Physics A, 79 (2004) 787–790.

Kuroda S., Kaihara S., Fujii Y., Kinoshita T., Adachi M., Modeling of particle generation in laser ablation plasma, Journal of Aerosol Science, 50 (2012) 38–56.

Lau M., Haxhiaj I., Wagener P., Intartaglia R., Brandi F., Nakamura J., Barcikowski S., Ligand-free gold atom clusters adsorbed on graphene nano sheets generated by oxidative laser fragmentation in water, Chemical Physics Letters, 610–611 (2014) 256–260.

Lu Q., Mao S.S., Mao X., Russo R.E., Theory analysis of wavelength dependence of laser-induced phase explosion of silicon, Journal of Applied Physics, 104 (2008) 083301.

Niu X., Murray P., Sarangan A., Synthesis of Fe–Ni bimetallic nanoparticles from pixel target ablation: Plume dynamics and surface characterization, Journal of Nanoparticle Research, 14 (2012) 1–8.

Okada R., Iijima S., Oxidation property of silicon small particles, Applied Physics Letters, 58 (1991) 1662–1663.

O'regan B., Gratzel M., A low-cost, high-efficiency solar cell based on dye-sensitized colloidal TiO2 films, Nature, 353 (1991) 737–740.

Orii T., Hirasawa M., Seto T., Tunable, narrow-band light emission from size-selected Si nanoparticles produced by pulsed-laser ablation, Applied Physics Letters, 83 (2003a) 3395–3397.

Orii T., Hirasawa M., Seto T., Aya N., Onari S., Temperature dependence of photoluminescence from mono-dispersed Si nanoparticles, The European Physical Journal D—Atomic, Molecular, Optical and Plasma Physics, 24 (2003b) 119–122.

Pallotti D.K., Ni X., Fittipaldi R., Wang X., Lettieri S., Vecchione A., Amoruso S., Laser ablation and deposition of titanium dioxide with ultrashort pulses at 527 nm, Applied Physics B, 119 (2015) 445–452.

Puretzky A.A., Geohegan D.B., Fan X., Pennycook S.J., Dynamics of single-wall carbon nanotube synthesis by laser vaporization, Applied Physics A, 70 (2000) 153–160.

Ruth A.A., Young J.A., Generation of CdSe and CdTe nanoparticles by laser ablation in liquids, Colloids and Surfaces A: Physicochem. Eng. Aspects, 279 (2006) 121–127.

Sakiyama K., Koga K., Seto T., Hirasawa M., Orii T., Formation of size-selected Ni/NiO core−shell particles by pulsed laser ablation, J. Phys. Chem. B, 108 (2004) 523–529.

Seto T., Kawakami Y., Suzuki N., Hirasawa M., Kano S., Aya N., Sasaki S., Shimura H., Evaluation of morphology and size distribution of silicon and titanium oxide nanoparticles generated by laser ablation, Journal of Nanoparticle Research, 3 (2001a) 185–191.

Seto T., Kawakami Y., Suzuki N., Hirasawa M., Aya N., Laser synthesis of uniform silicon single nanodots, Nano Letters,

1 (2001b) 315–318.
Seto T., Orii T., Hirasawa M., Aya N., Fabrication of silicon nanostructured films by deposition of size-selected nanoparticles generated by pulsed laser ablation, Thin Solid Films, 437 (2003) 230–234.
Seto T., Koga K., Akinaga H., Takano F., Sakiyama K., Hirasawa M., Orii T., Laser synthesis and magnetic properties of monodispersed core–shell nanoparticles, Applied Physics A, 79 (2004) 1165–1167.
Seto T., Akinaga H., Takano F., Koga K., Orii T., Hirasawa M., Magnetic properties of monodispersed Ni/NiO core−shell nanoparticles, The Journal of Physical Chemistry B, 109 (2005) 13403–13405.
Seto T., Koga K., Akinaga H., Takano F., Orii T., Hirasawa M., Laser ablation synthesis of monodispersed magnetic alloy nanoparticles, Journal of Nanoparticle Research, 8 (2006) 371–378.
Seto T., Koga K., Takano F., Akinaga H., Orii T., Hirasawa M., Murayama M., Synthesis of magnetic CoPt/$SiO_2$ nanoparticles, Journal of Physics: Conference Series, 59 (2007) 255–258.
Seto T., Inoue A., Higashi H., Otani Y., Kohno M., Hirasawa M., Phase transition and restructuring of carbon nanoparticles induced by aerosol laser irradiation, Carbon, 70 (2014) 224–232.
Shinde S.R., Kulkarni S.D., Banpurkar A.G., Nawathey-Dixit R., Date S.K., Ogale S.B., Magnetic properties of nanosized powders of magnetic oxides synthesized by pulsed laser ablation, Journal of Applied Physics, 88 (2000) 1566–1575.
Suzuki N., Makino T., Yamada Y., Yoshida T., Seto T., Monodispersed, nonagglomerated silicon nanocrystallites, Applied Physics Letters, 78 (2001) 2043–2045.
Tilke A.T., Simmel F.C., Blick R.H., Lorenz H., Kotthaus J.P., Coulomb blockade in silicon nanostructures, Progress in Quantum Electronics, 25 (2001) 97–138.
Torrisi L., Gammino S., Andò L., Nassisi V., Doria D., Pedone A., Comparison of nanosecond laser ablation at 1064 and 308 nm wavelength, Applied Surface Science, 210 (2003) 262–273.
Tsuji M., Seto T., Otani Y., Effect of surrounding gas temperature on the morphological evolution of $TiO_2$ nanoparticles generated by laser ablation in tubular furnace, Journal of Nanoparticle Research, 14 (2012) 674–683.
Wen S.B., Mao X., Greif R., Russo R.F., Radiative cooling of laser ablated vapor plumes: Experimental and theoretical analyses, Journal of Applied Physics, 100 (2006) 053104.
Wen S.B., Mao X., Greif R., Russo R.E., Experimental and theoretical studies of particle generation after laser ablation of copper with a background gas at atmospheric pressure, Journal of Applied Physics, 101 (2007) 123105.
Wolfbeis O.S., An overview of nanoparticles commonly used in fluorescent bioimaging, Chemical Society reviews, 44 (2015) 4743–4768.
Yoshida T., Takeyama S., Yamada Y., Mutoh K., Nanometer—sized silicon crystallites prepared by excimer laser ablation in constant pressure inert gas, Applied Physics Letters, 68 (1996) 1772–1774.
Yoshida T., Yamada Y., Orii T., Electroluminescence of silicon nanocrystallites prepared by pulsed laser ablation in reduced pressure inert gas, Journal of Applied Physics, 83 (1998) 5427–5432.
Zheng J., Zhang C., Dickson R.M., Highly fluorescent, water-soluble, size-tunable gold quantum dots, Physical Review Letters, 93 (2004) 077402.

## Author's short biography

**Myungjoon Kim**

He received his Bachelor of Science degree in Mechanical Engineering from Sungkyunkwan University, Korea in 2009. Currently, he is a candidate of combined master's and doctorate program in the School of Mechanical at Sungkyunkwan University. His research is focused on the numerical analysis on particle suspended in fluid.

## Author's short biography

**Saho Osone**

She received her Bachelor of Engineering degree in Chemical Engineering from Kanazawa University, Japan in 2007. She received her Master of Engineering in Chemical Engineering from Kanazawa University, Japan in 2009. Currently, she is working at Takeda Pharmaceutical Company Limited. She is also a doctoral course student at Kanazawa University. Her research in focused on nanoparticle material synthesis by gas phase processes and measurement of aerosol nanoparticles.

**Taesung Kim**

He received his Bachelor of Science degree in Mechanical Engineering from Seoul National University, Korea in 1994. He received his Master of Science, and Doctor of Philosophy degrees in Mechanical Engineering from Minnesota University, USA in 1998, and 2002, respectively. Dr. Kim currently works as professor in the School of Mechanical Engineering and adjunct professor in the SKKU Advanced Institute of Nano Technology at Sungkyunkwan University in Suwon, Korea. His research interests include nanoparticle synthesis, development of applications related with bio aerosol, Chemical Mechanical Polishing, and thin film synthesis.

**Hidenori Higashi**

He received his Bachelor of Engineering degree in Chemical Engineering from Kyushu University, Japan in 1994. He received his Master of Engineering, and Doctor of Engineering degrees in Chemical Engineering from Kyushu University, Japan in 1996, and 2001, respectively. From 1997 to 2004, he worked as a Research Associate at Kyushu University. From 2004, he works as an Assistant Professor (2004 to 2015) and as an Associate Professor (from 2016), Faculty of Natural System, Institute of Science and Engineering, Kanazawa University, Japan. His research topics cover broad area in supercritical fluid technology, aerosol science and technology.

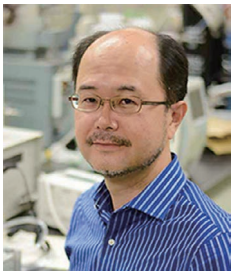

**Takafumi Seto**

He received the Doctoral degree in Engineering from Hiroshima University at 1996. From 1997 to 2007, he worked at Mechanical Engineering Laboratory (from 2001, National Institute of Industrial Science and Technology (AIST)). From 2007, he works as an Associate Professor (2007 to 2013) and as a Professor (2013 to now), Kanazawa University, Faculty of Natural System, Institute of Science and Engineering, Kanazawa University, Japan. His research topics cover broad area in aerosol science and technology such as nanoparticle synthesis, classification, transport phenomena, electrostatics, instrumentation, and laser ablation.